coatings

MDPI

Article

Influence of Annealing Temperature on the Properties of $ZnGa_2O_4$ Thin Films by Magnetron Sputtering

Wei-Kai Wang [1,*], Kuo-Feng Liu [2], Pi-Chuen Tsai [2], Yi-Jie Xu [1] and Shih-Yung Huang [3]

[1] Department of Materials Science and Engineering, Da-Yeh University, Changhua 51591, Taiwan; pa821221@yahoo.com.tw

[2] Graduate Institute of Materials Science and Green Energy Engineering, National Formosa University, Huwei, Yunlin 632, Taiwan; david0802david0802@gmail.com (K.-F.L.); pc6996@ms16.hinet.net (P.-C.T.)

[3] Department of Industrial Engineering and Management, Da-Yeh University, Changhua 51591, Taiwan; syh@mail.dyu.edu.tw

* Correspondence: wk@mail.dyu.edu.tw; Tel.: +886-4-8511-888 (ext. 2606)

Received: 16 November 2019; Accepted: 11 December 2019; Published: 14 December 2019

Abstract: Zinc gallate ($ZnGa_2O_4$) thin films were grown on sapphire (0001) substrate using radio frequency (RF) magnetron sputtering. After the thin film deposition process, the grown $ZnGa_2O_4$ was annealed at a temperature ranging from 500 to 900 °C at atmospheric conditions. The average crystallite size of the grown $ZnGa_2O_4$ thin films increased from 11.94 to 27.05 nm as the annealing temperature rose from 500 to 900 °C. Excess Ga released from $ZnGa_2O_4$ during thermal annealing treatment resulted in the appearance of a Ga_2O_3 phase. High-resolution transmission electron microscope image analysis revealed that the preferential crystallographic orientation of the well-arranged, quasi-single-crystalline $ZnGa_2O_4$ (111) plane lattice fringes were formed after the thermal annealing process. The effect of crystallite sizes and lattice strain on the width of the X-ray diffraction peak of the annealed $ZnGa_2O_4$ thin films were investigated using Williamson-Hall analysis. The results indicate that the crystalline quality of the deposited $ZnGa_2O_4$ thin film improved at higher annealing temperatures.

Keywords: thin film; magnetron sputtering; microstructure; $ZnGa_2O_4$; annealing

1. Introduction

Zinc gallate ($ZnGa_2O_4$) belongs to a group of close-packed, face-centered cubic structured compounds (AB_2O_4) with a normal oxide spinel structure (space group of Fd3m). Zn^{2+} and Ga^{3+} cations occupy the tetrahedrally coordinated A-sites in tetrahedral and octahedral lattice B-sites, respectively. The lattice constant is 8.334 Å at room temperature [1]. $ZnGa_2O_4$ materials have recently gained increased attention [2,3]. These materials are widely applied in vacuum fluorescent and field emission displays, gas sensors, electronic devices, and solar-blind ultraviolet photodetectors (PDs) due to their high transparency in the deep ultraviolet (DUV) spectral region, excellent thermal and chemical stability, and wide optical band gap (~5 eV) [4–6].

Researchers have discussed many one-dimensional (1D) $ZnGa_2O_4$ nanostructures (nanoparticles, nanocrystal, nanowires, and nanotube) over the years [7–9]. Although these 1D $ZnGa_2O_4$ devices exhibit high optoelectronic performance, the reliability and stability of these devices are a critical aspect of their application, which raises concern [10,11]. Thin film structures have been proven to possess properties that can overcome the aforementioned challenges posed by a 1D $ZnGa_2O_4$ nanostructure. Therefore, it is important to develop and perfect $ZnGa_2O_4$ film materials and related optoelectronic devices.

There are several methods for the preparation of $ZnGa_2O_4$ thin films, including: sol-gel [12], pulsed laser deposition [13], metalorganic chemical vapor deposition (MOCVD) [14], and radio

frequency (RF) magnetron sputtering [15]. Shen et al. used $ZnGa_2O_4$ thin film for the development of metal-oxide-semiconductor field effect transistors by MOCVD. Their research showed promising results in enhancing the breakdown voltage and I_{on}/I_{off} (current on/off) ratio performance [16]. Wu et al. reported that the properties of thin film $ZnGa_2O_4$ gas sensor deposited by MOCVD [17]. Huang et al. developed a $ZnGa_2O_4$ thin film solar-blind PDs based on a metal-semiconductor-metal structure fabricated by an RF magnetron sputtering method [18]. They investigated the effect of oxygen partial pressure on the electrical properties of the devices during the sputtering and thermal annealing process.

Among these growth techniques, RF magnetron sputtering techniques have many advantages, including the ease of controlling the growth parameter, excellent packing density, good adhesion, and relatively low running cost. However, the RF magnetron sputtering method often produces amorphous or polycrystalline film structures that significantly destroy the optical and electrical properties of the material. Enhancement of polycrystalline thin films has spurred several types of research, leading to the investigation of process parameters that include growth temperature, film thickening, post-annealing temperature, and RF power. In this paper, the effects of post-annealing temperatures on the structural and optical properties of $ZnGa_2O_4$ films deposited on sapphire substrates after RF magnetron sputtering were investigated.

2. Experimental Methods

The $ZnGa_2O_4$ thin films were deposited over a C-plane sapphire using the RF magnetron sputtering technique. The sputtering target was $ZnGa_2O_4$ ceramic, which was sintered with ZnO and Ga_2O_3 powder of 99.99% purity, with a mix proportion of 30:70. Initially, the substrates were cleaned in acetone and alcohol, followed by ultrasonic cleansing in de-ionized water for 10 min, and then blow-dried with nitrogen gas. Prior to deposition, the vacuum level of chamber pressure was approximately 5×10^{-6} torr. The plasma generation was activated by the RF power for $ZnGa_2O_4$, the target was 150 W at 13.56 MHz, and the deposition pressure was kept at 5×10^{-3} torr. The as-deposited film was deposited at the substrate temperature of 400 °C. The distance between target and the substrate was 15 cm. To maintain uniform film thickness, the substrate holder was rotated at 18 rpm during the deposition process. The deposition time was 2 h and the deposited samples were annealing at different temperature ranging from 500 to 900 °C in steps of 100 °C at atmospheric ambient conditions in a quartz furnace tube. The crystallographic properties of $ZnGa_2O_4$ films were investigated by X-ray diffraction (XRD, X'Pert PRO MRD, PANalytical, Almelo, The Netherlands) with Cu Kα X-ray source (λ = 1.541874 Å) radiation. The surface morphologies, microstructures, and elemental analyses of these deposited samples were analyzed by scanning electron microscopy (SEM, S-3000H, Hitachi, Tokyo, Japan), atomic force microscopy (AFM, 5400, Agilent, Santa Clara, CA, USA), and high-resolution transmission electron microscopy (HRTEM, H-600, Hitachi, Tokyo, Japan). Optical properties (transmittance, absorbance, and photoluminescence) were determined using an UV-visible (UV-VIS) near infra-red (NIR) spectrophotometer (Model: LAMBDA 750 from Perkin Elmer, Perkin Elmer, MA, USA).

3. Results

The XRD spectra of the deposited $ZnGa_2O_4$ thin films as a function of annealing temperature is shown in Figure 1a. The annealing temperature was varied from 500 to 900 °C for 1 h. The polycrystalline nature of all the deposited $ZnGa_2O_4$ film can be indexed and refer to the reported data of Joint Committee on Powder Diffraction Standards (JCPDS) card file 38-1240; the characteristic peaks of the preferred crystallographic orientations are (220), (311), (222), (400), (511), and (440). The intensity of the diffraction peak (311) plane increased with an increase in the annealing temperature. The increment of the diffraction peak (311) is attributed to improved crystallinity of deposited $ZnGa_2O_4$ thin films. The diffraction peaks of Ga_2O_3 (−401) and (−202) were observed from the phase separation of $ZnGa_2O_4$ for the sample annealed at a temperature above 800 °C (Figure 1b). The JCPDS data of the Ga_2O_3 (card No. 43-1012) is given for reference. The observed Ga_2O_3 plane is attributed to the expulsion of Zn atoms at an annealing temperature above 800 °C [19]. The Debye-Scherrer formula in Equation (1)

below was used to calculate the average crystallite size and full width at half maxima (FWHM) of $ZnGa_2O_4$ peak (311) at different annealing temperatures, as shown in Figure 1c [20]:

$$D = 0.9\lambda/\beta\cos\theta \quad (1)$$

where D is the average crystallite size (nm), λ is the wavelength of X-ray (0.15418 nm), β is the FWHM (radian), and θ is diffraction angle (degrees). The average crystallite sizes estimated by the Scherrer method increase from 11.94 to 27.05 nm. $ZnGa_2O_4$ crystallite size increased with an increase in annealing temperatures, and a narrower FWHM peak (311) was observed, indicating an improvement in the crystallinity of $ZnGa_2O_4$ (Figure 1c). The observation might be due to the enhanced nucleation dynamics and/or strain release. Based on the solid-state diffusion process, either the aggregation of small grains to form larger ones, or grain boundary movement, results in grain recrystallization and regrowth. This improved the crystallinity of $ZnGa_2O_4$ film at high annealing temperatures [21].

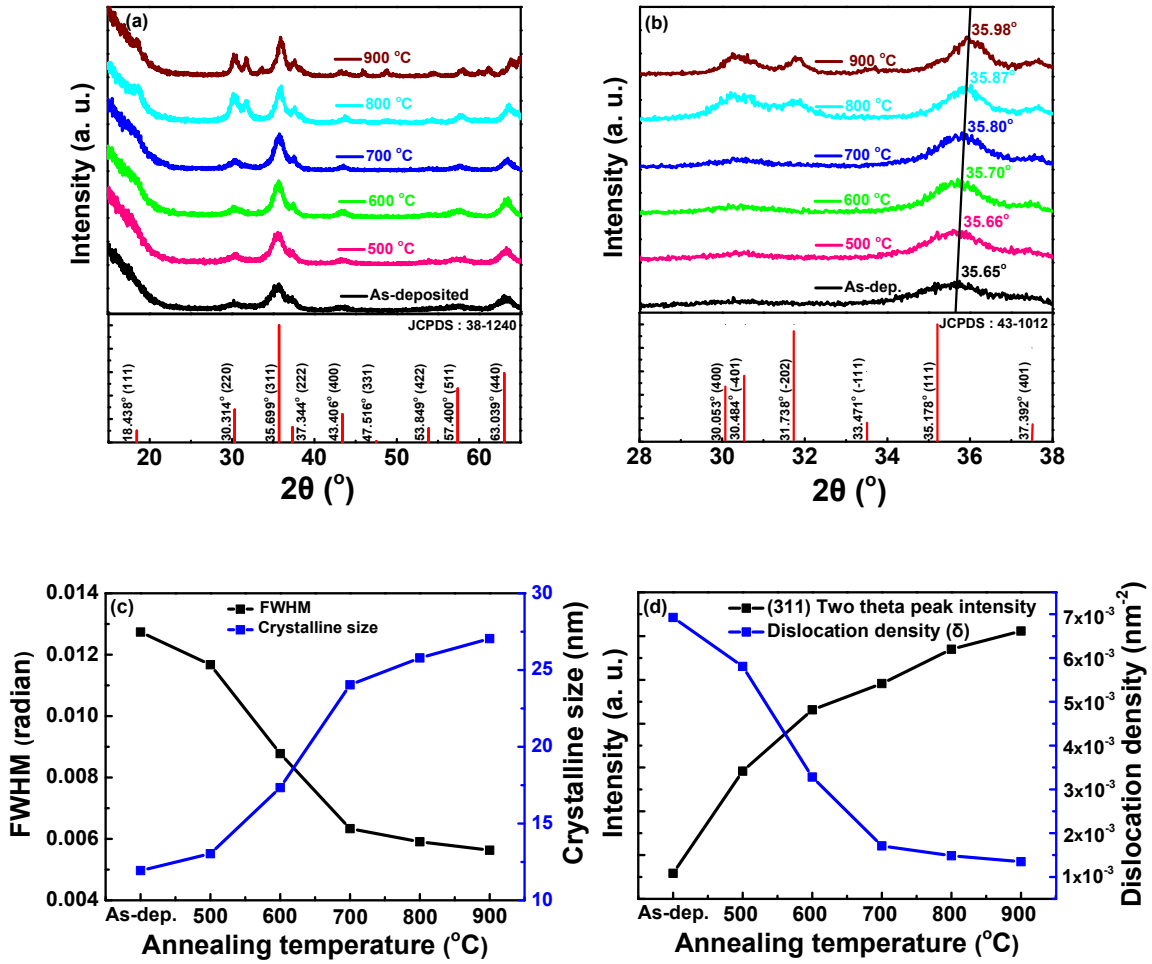

Figure 1. (**a**) XRD spectra of $ZnGa_2O_4$ films at different annealing temperatures; (**b**) XRD spectra of $ZnGa_2O_4$ showing a limited 2θ range (28° to 38°); (**c**) Effect of annealing temperature on the average crystallite size and FWHM of $ZnGa_2O_4$; (**d**) Effect of annealing temperature on the XRD peak intensity (311) and dislocation density.

Figure 1d shows the variation of XRD peak intensity (311) and dislocation density with increased annealing temperatures. The value of the dislocation density (δ), which is related to the number of defects in the grown nanocrystalline film, was calculated from the average values of the crystallite size by the relationship in Equation (2) [22]:

$$\delta = 1/D^2 \quad (2)$$

The dislocation density decreases as the annealing temperature increases, resulting in a decrement in the nature of native imperfections (defects, concentration of native impurity, and stress) at high annealing temperatures [23]. The Williamson-Hall analysis was used to evaluate the crystalline sizes and lattice strain distribution in the sample. This can be determined by Equation (3) [24]. The calculated parameters are shown in Table 1.

$$\beta_{hkl}\cos(\theta_{hkl}) = k\lambda/D_{W\text{-}H} + 4\varepsilon\sin(\theta_{hkl}) \quad (3)$$

where ε is the lattice strain, k is the shape factor, and (hkl) is the Miller Indices. Other parameters have previously been defined in Equation (1). The strain in the $ZnGa_2O_4$/sapphire samples at different annealing temperatures can be calculated from the slope of plotted of $\beta_{hkl}\cos\theta_{hkl}$ (along the y-axis) and $\sin\theta$ (along the x-axis) as shown in Figure 2a–f. The slopes of the fitted trendline for each plot (Figure 2a–e) were negative, indicating the existence of compressive strain in the lattice of all $ZnGa_2O_4$/sapphire samples. The intrinsic compressive stresses observed in the sputtering method deposited films were mainly caused by energetic particle bombardment, lattice mismatch, defects, etc. of the depositing films/substrate. After the sample was annealed at 900 °C, a positive slope was observed, which indicates the existence of tensile strain in the lattice (Figure 2f) [25].

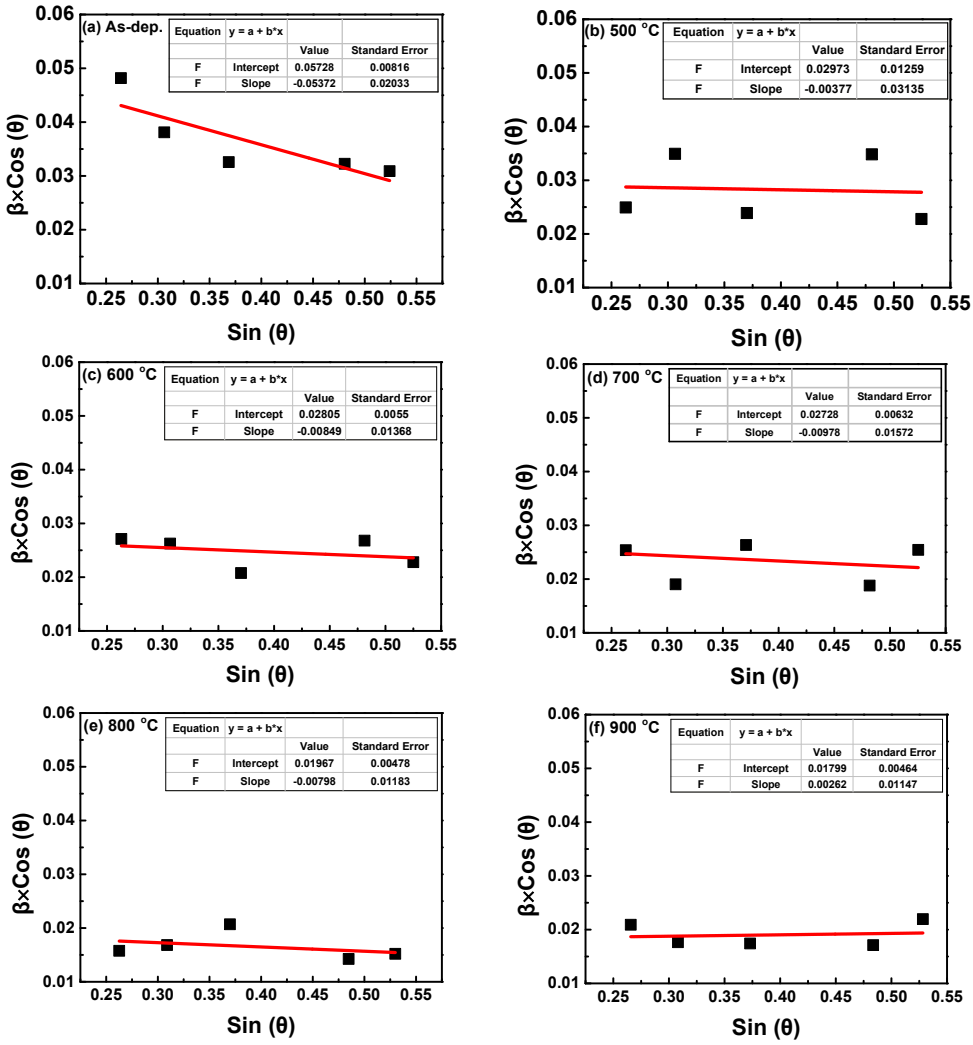

Figure 2. Williamson-Hall plot for $ZnGa_2O_4$ thin films annealed at temperature of (**a**) as-deposited, (**b**) 500 °C, (**c**) 600 °C, (**d**) 700 °C, (**e**) 800 °C, and (**f**) 900 °C.

Table 1. The crystallite size (*D*), dislocation density (δ) and energy bandgap for $ZnGa_2O_4$ thin films annealed at different temperature.

Temperature	Scherrer's Method		Williamson-Hall			Energy Gap (eV)
	D (mm)	$\delta \times 10^{15}$	*D* (mm)	$\delta \times 10^{15}$	$\varepsilon \times 10^{-3}$	
As-deposited	11.94	6.93	13.40	5.57	53.7	4.69
500 °C	13.04	5.80	14.64	4.66	3.77	4.77
600 °C	17.34	3.28	19.22	2.71	8.49	4.80
700 °C	24.03	1.71	26.98	1.37	9.78	4.86
800 °C	25.79	1.48	28.98	1.19	7.98	4.92
900 °C	27.05	1.35	30.43	1.08	2.62	4.98

Plane-view SEM images of the $ZnGa_2O_4$ films at different annealing temperatures are shown in Figure 3a–f. It can be seen that the surface morphologies of these $ZnGa_2O_4$ films exhibit a very similar column structure. As the annealing temperature increases, the crystallite size increases. The increment is caused by regrowth and coalescence during thermal treatment. Moreover, a high annealing temperature provides sufficient driving force to improve the mobility of the atoms, and further improve the film crystallinity. These results are in agreement with the observation from the XRD spectra. It can be concluding that the crystallinity of the films can be improved by controlling annealing temperature. Similar results have been reported by Sharma et al. [26].

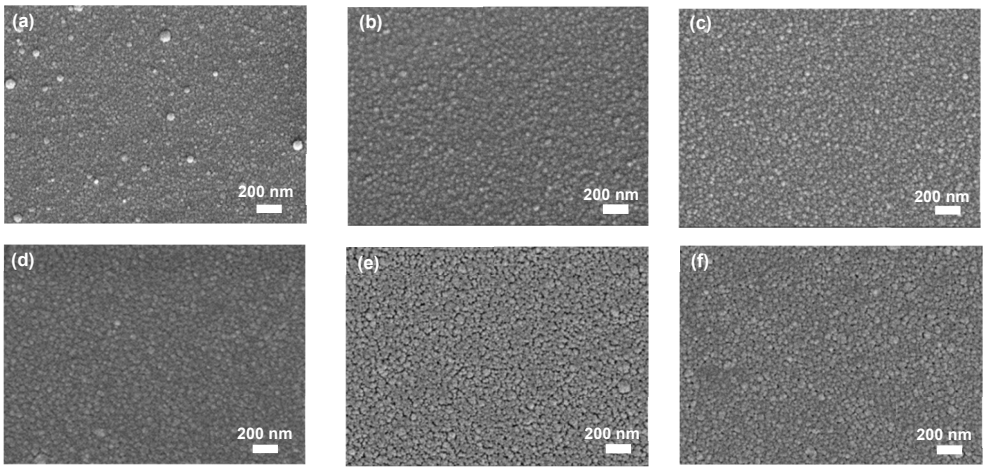

Figure 3. SEM micrographs of $ZnGa_2O_4$ thin film samples at different annealing temperatures of (**a**) as-deposited, (**b**) 500 °C, (**c**) 600 °C, (**d**) 700 °C, (**e**) 800 °C, and (**f**) 900 °C.

The surface morphologies of the $ZnGa_2O_4$ films at various annealing temperatures were obtained by AFM, as shown in Figure 4. The root mean square (RMS) values of the annealed samples (500, 600, and 700 °C) decreased compared to that of the as-deposited sample. As the annealing temperature increased above 800 °C, the RMS increased from 3.228 to 3.549 nm. This can be attributed to the phase separation that occurred at the surface resulting from the thermal decomposition or atomic migration on the disordered nanostructure of the $ZnGa_2O_4$ film. Figure 5a shows the cross-sectional transmission electron microscopy (TEM) images of $ZnGa_2O_4$ film annealed at a temperature of 900 °C. It was found that the $ZnGa_2O_4$ film exhibited a columnar structure with a thickness of approximately 485 nm. To investigate the detailed microstructure and compositional distribution of annealed $ZnGa_2O_4$ films, zones I, II, and III in Figure 5a were further analyzed by HRTEM. D-spacing was used to define the distance between planes of atoms in crystalline materials. Nanocrystalline grains including the crystal planes of $ZnGa_2O_4$ (311) and Ga_2O_3 (−401) were observed (Figure 5b), which corresponded to a d-spacing of 2.5 and 2.9 Å, respectively. This is because Zn atoms diffuse from the film at high annealing temperatures resulting in the partial conversion of $ZnGa_2O_4$ to Ga_2O_3. Therefore, it can be

inferred that the Ga_2O_3 phases are accompanied by $ZnGa_2O_4$ phases in this layer. Multiple phases including $ZnGa_2O_4$ (311), (222), (400), and (220) plane were obtained, as shown in Figure 5c. The clear crystal lattice stripes with the preferred orientation perpendicular to the film surface of cubic $ZnGa_2O_4$ (111) (d-spacing value of 4.8 Å) possess a quasi-single-crystalline structure (Figure 4d). This result might be attributed to the thermally activated process that provides enough kinetic energy, which was imparted to the $ZnGa_2O_4$ molecules. The imparted kinetic energy aids the rearrangement and improvement of crystallite perfection in the $ZnGa_2O_4$ thin film structure.

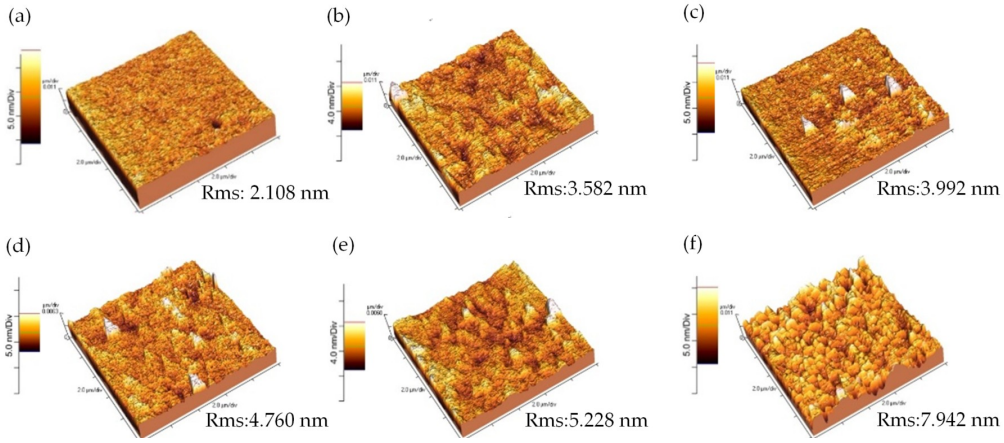

Figure 4. AFM images of $ZnGa_2O_4$ films annealed at different temperatures of (**a**) as-deposited, (**b**) 500 °C, (**c**) 600 °C, (**d**) 700 °C, (**e**) 800 °C, and (**f**) 900 °C.

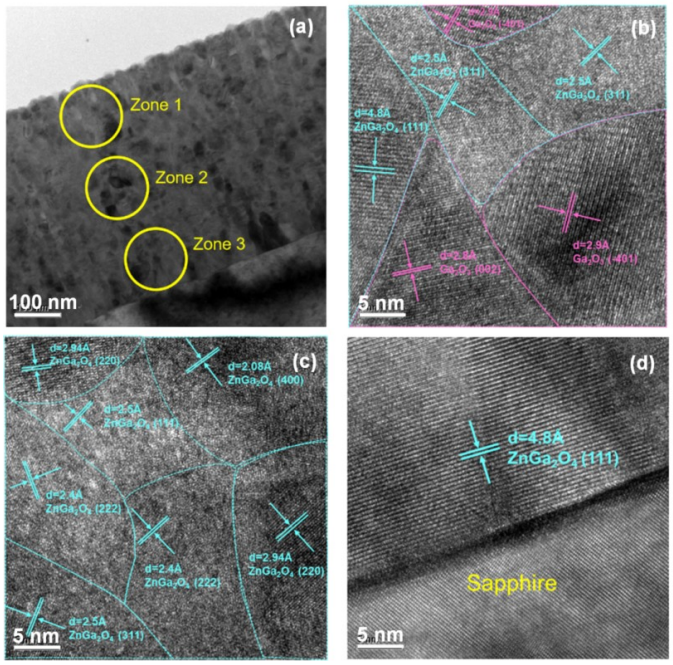

Figure 5. (**a**) Cross-sectional TEM image of the $ZnGa_2O_4$/sapphire sample. HRTEM images focused on (**b**) Zone 1, (**c**) Zone 2, and (**d**) Zone 3.

The optical transmittance spectra and energy gap of $ZnGa_2O_4$ films annealed at different temperatures are shown in Figure 6. The optical transmittance spectra of $ZnGa_2O_4$ thin films were recorded from 200 to 1000 nm. All deposited $ZnGa_2O_4$ films showed high transmittance greater than 80% in the ultraviolet A radiation UVA (400–315 nm) and ultraviolet B radiation (UVB) (315–280 nm) regions. The decrease may be attributed to a rough surface, as observed in the AFM result. The energy gap of $ZnGa_2O_4$ thin films at annealing temperatures ranging from 500 to 900 °C can be evaluated

from the absorption edge $(\alpha h\nu)^2$ curve as shown in Figure 6b [27], where α is the absorption coefficient and $h\nu$ is the photon energy. The photon energy gap increased from 4.7 eV for the as-deposited sample to 4.98 eV as the annealing temperature increased to 900 °C. The increase in energy gap is attributed to the decrease in the number of defect densities and grain boundaries, as well as the increase in the annealing temperature. The energy gap is narrowed because the amorphous structure usually produces excited electrons that undergo conduction in defect state [28].

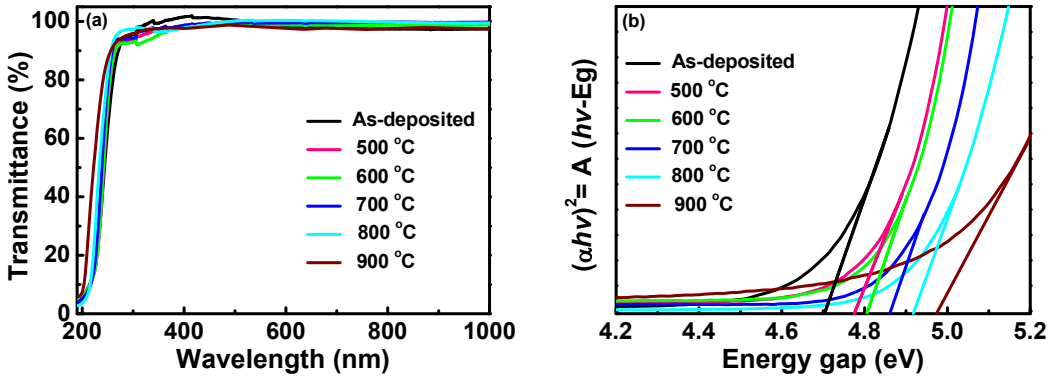

Figure 6. (**a**) Optical transmittance plot of $ZnGa_2O_4$ films at various annealing temperatures and (**b**) $(\alpha h\nu)^2$ versus energy gap plot for optical bandgap calculation.

The photoluminescence emission spectra of $ZnGa_2O_4$ thin films at various annealing temperature is shown in Figure 7a. It was observed that the sample under higher annealing temperatures has a higher luminescence intensity. While all of the annealed samples of photoluminescence spectra exhibited broad band emission extending from 300 to 600 nm, the emission peaks were located at 340 and 520 nm. The emission peak centered at 340 nm can be attributed to the $^4T_{2B} \rightarrow {}^4T_{2A}$ transition, while the $^2E_A \rightarrow {}^4T_{2A}$ transition is responsible for the emission peak centered at 520 nm. Since the UV band emission is related to the excited excess Ga^{3+} ions of the Ga–O group [29]. During thermal annealing, the Ga^{3+} ions substitute the Zn^{2+} ions site in the AB_2O_4 spinel structure, then interactions between the *p* orbitals in the Ga^{3+} ion and the orbitals of the six oxygen ligands lead to a shifts in the energy levels of the individual orbitals in a distorted octahedral configuration, further splitting the five 3*d*-orbital energy levels. The five 3*d*-orbital energy levels are labeled $^4T_1$, $^4T_{2A}$, $^4T_{2B}$, ^2E_B, ^2E_A, and $^4A_2$. A schematic diagram of the energy levels in $ZnGa_2O_4$ thin films is illustrated in Figure 7b. It was previously reported that $ZnGa_2O_4$ annealed at different temperatures may lead to transitions as a result of the stoichiometric variations in the composition of Ga/Zn [30]. The possibility of the expulsion of Zn atoms from the $ZnGa_2O_4$ matrix increases with an increase in the annealing temperature. Therefore, a variation in the Ga/Zn stoichiometry in $ZnGa_2O_4$ thin films will be observed.

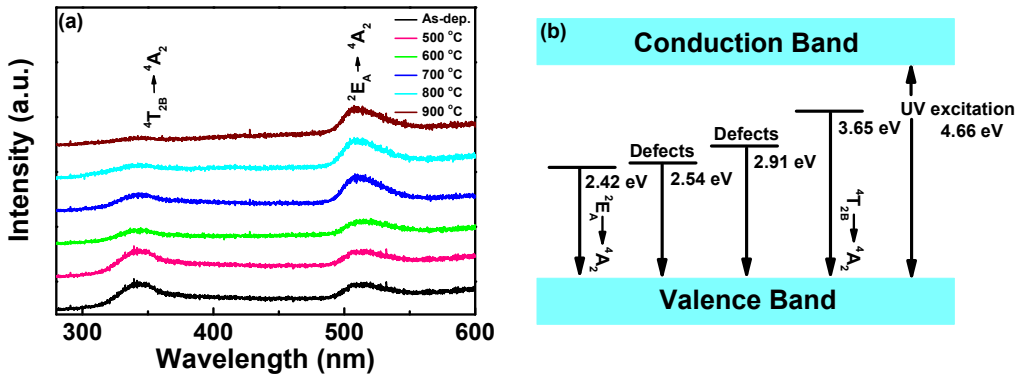

Figure 7. (**a**) Photoluminescence spectra of $ZnGa_2O_4$ films annealed at different temperatures and (**b**) energy levels diagram in $ZnGa_2O_4$ film.

4. Conclusions

In this study, $ZnGa_2O_4$ thin films were prepared on sapphire substrate using an RF sputtering technique. The polycrystalline nature of the randomly oriented $ZnGa_2O_4$ films was improved and converted to a quasi-single-crystalline structure through thermal annealing treatment. The stress of the deposited $ZnGa_2O_4$ thin films was transformed from compressive to tensile stress as the annealing temperature increased from 500 to 900 °C. The optical transmittance of $ZnGa_2O_4$ films was greater than 80% in the UVA and UVB regions, and the energy band gap increased with an increase in annealing temperature. These results indicate that the annealing process is an effective method for the improvement of $ZnGa_2O_4$ thin film crystallinity, and may obtain the preferred orientation.

Author Contributions: Conceptualization, W.-K.W.; Methodology, Y.-J.X., S.-Y.H., K.-F.L., P.-C.T. and W.-K.W.; Data Curation, Y.-J.X., K.-F.L. and W.-K.W.; Writing—Original Draft Preparation, Y.-J.X., K.-F.L. and W.-K.W.; Writing—Review and Editing, W.-K.W.

Funding: This research was funded by the Ministry of Science and Technology, Taiwan (No. 108-2221-E-212-007).

Acknowledgments: The authors wish to express their sincere gratitude for the technical support from the advanced Industry Technology Centre of National Chung Hsing University, Taiwan.

Conflicts of Interest: The authors declare no conflict of interest.

References

1. Omata, T.; Ueda, N.; Ueda, K.; Kawazoe, H. New ultraviolet-transport electroconductive oxide, $ZnGa_2O_4$ spinel. *Appl. Phys. Lett.* **1994**, *64*, 1077–1078. [CrossRef]
2. Tsai, S.H.; Shen, Y.C.; Huang, C.Y.; Horng, R.H. Deep-ultraviolet Schottky photodetectors with high deep-ultraviolet/visible rejection based on a $ZnGa_2O_4$ thin film. *Appl. Surf. Sci.* **2019**, *496*, 143670. [CrossRef]
3. Lee, H.; Bark, C.W.; Choi, H.W. Fabrication and characterization of perovskite solar cells with $ZnGa_2O_4$ mixed TiO_2 photoelectrode. *Jpn. J. Appl. Phys.* **2019**, *58*, SDDE15. [CrossRef]
4. Horng, R.H.; Huang, C.I.; Ou, H.L.; Juang, T.K.; Liu, P.L. Epitaxial growth of $ZnGa_2O_4$: A new, deep ultraviolet semiconductor candidate. *Cryst. Growth Des.* **2017**, *17*, 6071–6078. [CrossRef]
5. Jiao, Z.; Ye, G.; Chen, F.; Li, M.; Liu, J. The preparation of $ZnGa_2O_4$ nano crystals by spray coprecipitation and its gas sensitive characteristics. *Sensors* **2002**, *2*, 71–78. [CrossRef]
6. Lee, Y.E.; Norton, D.P.; Budai, J.D.; Wei, Y. Enhanced ultraviolet photoconductivity in semiconducting $ZnGa_2O_4$ thin films. *J. Appl. Phys.* **2001**, *90*, 3863. [CrossRef]
7. Kamal, C.S.; Boddu, S.; Vishwanadh, B.; Rao, K.R.; Sudarsan, V.; Vatsa, R.K. Blue luminescence from $ZnGa_2O_4$: Effect of lattice distortion and particle size. *J. Lumin.* **2017**, *188*, 429–435. [CrossRef]
8. Liang, H.F.; Meng, F.; Lamb, B.K.; Ding, Q.; Li, L.S.; Wang, Z.C.; Jin, S. Solution growth of screw dislocation driven alpha-GaOOH nanorod arrays and their conversion to porous $ZnGa_2O_4$ nanotubes. *Chem. Mater.* **2017**, *29*, 7278–7287. [CrossRef]
9. Hirano, M.; Okumura, S.; Hasegawa, Y.; Inagaki, M. Direct precipitation of spinel type oxide $ZnGa_2O_4$ from aqueous solutions at low temperature below 90 °C. *Inorg. Mater.* **2001**, *3*, 797–801. [CrossRef]
10. Lou, Z.; Li, L.; Shen, G. High-performance rigid and flexible ultraviolet photodetectors with single-crystalline $ZnGa_2O_4$ nanowires. *Nano Res.* **2015**, *8*, 2162–2169. [CrossRef]
11. Li, C.; Bando, Y.; Liao, M.; Koide, Y.; Golberg, D. Visible-blind deep-ultraviolet schottky photodetector with a photocurrent gain based on individual Zn_2GeO_4 nanowire. *Appl. Phys. Lett.* **2010**, *97*, 161102. [CrossRef]
12. Hussen, M.K.; Dejene, F.B.; Gonfa, G.G. Effect of citric acid on material properties of $ZnGa_2O_4$:Cr^{3+} nanopowder by sol-gel method. *Appl. Phys. A Mater.* **2018**, *124*, 390. [CrossRef]
13. Shi, Q.; Wang, C.Z.; Zhang, D.; Li, S.H.; Zhang, L.M.; Wang, W.J.; Zhang, J.Y. Luminescence of Cr^{3+} doped $ZnGa_2O_4$ thin films deposited by pulsed laser ablation. *Thin Solid Film.* **2012**, *520*, 6845–6849. [CrossRef]
14. Lina, X.; Chen, D.; Niu, W.; Huang, C.Y.; Horng, R.H.; Cheng, L.C.; Talwar, D.N.; Lin, H.H.; Lee, J.F.; Feng, Z.C.; et al. Evolution of the local structure and crystal phase for thin ZnGaO films grown by metal organic chemical vapor deposition. *J. Cryst. Growth* **2019**, *520*, 89–95. [CrossRef]

15. Wang, W.K.; Xu, Y.J.; Huang, S.Y.; Liu, K.F.; Tsai, P.C. Structural characteristics and photoluminescence properties of sputter-deposition $ZnGa_2O_4$ thin films on sapphire and Si(100) substrates. *Coatings* **2019**, *9*, 469. [CrossRef]
16. Shen, Y.S.; Wang, W.K.; Horng, R.H. Characterizations of metal-oxide-semiconductor field-effect transistors of ZnGaO grown on sapphire substrate. *IEEE J. Electron Devices Soc.* **2017**, *5*, 112–116. [CrossRef]
17. Wu, M.R.; Li, W.Z.; Tung, C.Y.; Huang, C.Y.; Chiang, Y.H.; Liu, P.L.; Horng, R.H. NO gas sensor based on $ZnGa_2O_4$ epilayer grown by metalorganic chemical vapor deposition. *Sci. Rep.* **2019**, *9*, 7459. [CrossRef]
18. Huang, W.L.; Li, C.H.; Chang, S.P.; Chang, S.J. The Effect of oxygen partial pressure and annealing process on the characteristics of $ZnGa_2O_4$ MSM UV photodetector. *ECS J. Solid State Sci. Technol.* **2019**, *8*, Q3213–Q3216. [CrossRef]
19. Yi, S.S.; Bae, J.S.; Moon, B.K.; Jeong, J.H.; Kim, I.W.; Park, H.L. Photoluminescence behavior of pulsed laser deposited $ZnGa_2O_4$ thin-film phosphors grown on various substrates. *Appl. Phys. A* **2003**, *76*, 433–437. [CrossRef]
20. Chandolu, A.; Nikishin, S.; Holtz, M.; Temkin, H. X-ray diffraction study of AlN/AlGaN short period superlattices. *J. Appl. Phys.* **2007**, *102*, 114909. [CrossRef]
21. Lee, J.Y.; Kim, H.S.; Chang, J.H.; Yang, M.; Ahn, H.S.; Ryu, S.O. Structural and luminescence characteristics of post-annealed ZnO films on Si (111) in H_2O ambient. *Jpn. J. Appl. Phys.* **2005**, *44*, L205–L207. [CrossRef]
22. Sharma, S.; Vyas, S.; Periasamy, C.; Chakrabarti, P. Structural and optical characterization of ZnO thin films for optoelectronic device applications by RF sputtering technique. *Superlattices Microstruct.* **2014**, *75*, 378–389. [CrossRef]
23. Son, H.; Choi, Y.J.; Hwang, J.; Jeon, D.W. Influence of post-annealing on properties of α-Ga_2O_3 epilayer. *ECS J. Solid State Sci. Technol.* **2019**, *8*, Q3024–Q3027. [CrossRef]
24. Zak, A.K.; Majid, W.H.A.; Abrishami, M.E.; Yousefi, R. X-ray analysis of ZnO nanoparticles by Williamson–Hall and size-strain plot methods. *Solid State Sci.* **2011**, *13*, 251–256.
25. Somasundaram, K.; Abhilash, K.P.; Sudarsan, V.; Christopher Selvin, P.; Kadam, R.M. Defect luminescence and lattice strain in Mn^{2+} doped $ZnGa_2O_4$. *Phys. B* **2016**, *491*, 79–83. [CrossRef]
26. Sharma, S.; Varma, T.; Asokan, K.; Periasamy, C.; Boolchandani, D. Annealing temperature dependent structural and optical properties of RF sputtered ZnO thin films. *J. Nanosci. Nanotechnol.* **2017**, *17*, 300–305. [CrossRef]
27. Shi, F.F.; Han, J.; Xing, Y.H.; Li, J.H.; Zhang, L.; He, T.; Li, T.; Deng, X.U.; Zhang, X.D.; Zhang, B.H. Annealing effects on properties of Ga_2O_3 films deposited by plasma-enhanced atomic layer deposition. *Mater. Lett.* **2019**, *237*, 105–108. [CrossRef]
28. Chen, P.W.; Huang, S.Y.; Yuan, S.H.; Chen, Y.A.; Hsiao, P.W.; Wuu, D.S. Quasi-single-crystalline $ZnGa_2O_4$ films via solid phase epitaxy for enhancing deep-ultraviolet photoresponse. *Adv. Mater. Interfaces* **2019**, *6*, 1901075. [CrossRef]
29. Hsieh, I.J.; Chu, K.T.; Yu, C.F.; Feng, M.S. Cathodoluminescent characteristics of $ZnGa2O_4$ phosphor grown by radio frequency magnetron sputtering. *J. Appl. Phys.* **1994**, *76*, 3735–3739. [CrossRef]
30. Lee, Y.E.; Norton, D.P.; Park, C.; Rouleau, C.M. Blue photoluminescence in $ZnGa_2O_4$ thin-film phosphors. *J. Appl. Phys.* **2001**, *89*, 1653–1656. [CrossRef]